AIAA SciTech Forum
23-27 January 2023, National Harbor, MD & Online
AIAA SCITECH 2023 Forum

10.2514/6.2023-1407

Plume-Material Interactions of Metallic Surfaces Bombarded by an [EMIM][BF_4] Electrospray Source

Avinash Rao[1], Tanapat Bhakyapaibul[2], Joshua L. Rovey[3], Deborah Levin[4], and Huck Beng Chew[5]
University of Illinois Urbana-Champaign, Urbana, IL, 61801, USA

Experiments conducted at the University of Illinois Urbana-Champaign Electric Propulsion Laboratory investigated the effects of surface finish and vacuum baking on secondary charged species yield from metallic surfaces bombarded by a plume from a fundamental electrospray source utilizing [EMIM][BF_4]. Cation induced positive charge yields for aluminum ranged from 0.1 to 0.4 charges per incident ion and cation induced negative charge yields ranged from 0 to 0.5 charges per incident ion. Anion induced positive charge yields for the same material were low enough to effectively be 0, while anion induced negative charge yields ranged from 1 to 1.4 charges per incident ion. For stainless steel, cation induced positive charge yields varied from 0.1 to 0.3 charges per incident ion and cation induced positive charge yields ranged from 0.1 to 0.2 charges per incident ion. As with the aluminum, the anion induced positive charge yield was low enough so as to be 0, while the anion induced negative charge yield ranged from 0.9 to 1.3 charges per incident ion. The variance did not appear to result from the emitter voltage, nor did the surface finish seem to have any definitive effect on the yields. Variance in the data may arise from currently uncontrolled variations within the plume ions such as angle-of-incidence and plume current density. As a precursor to modeling similar experimental setups through molecular dynamics or with particle-in-cell methods, simulations of 1,000 all-atom [EMIM][BF_4] molecules were developed to characterize the response of an ionic liquid to the presence of an electric field. When an electric field of 6 V/nm was applied to the entire simulation domain, the number and variety of emitted species increased from 2 to 4 to 13 for 100 ps, 200 ps, and 1,000 ps, respectively.

I. Introduction

Electrospray thrusters are a type of electrostatic propulsion device that provides thrust by accelerating droplets or ions of ionic liquids (IL) to high velocities. In recent years, electrospray propulsion has been investigated as an attractive candidate for small satellites and deep space missions. One challenge in evaluating electrospray propulsion for use on spacecraft are potential interactions between the electrospray plume and nearby surfaces, whether in facilities in ground tests or on-board spacecraft. Recent work evaluating electrospray thruster performance and spacecraft charging effects noted anomalous charge loss as well as mass loss from elements downstream of the thruster [1, 2]. Semi-empirical models using TRansport of Ions in Matter (TRIM) subroutines have also noted that the specific secondary charged species yield varies with the incoming energy and velocity of primary polyatomic ions [3]. These deficits in charge measurements influence plume diagnostics collected, which are then used to calculate and predict thruster performance, potentially leading to inaccurate assessments of propulsive capabilities. Prior work done at the University of Illinois has previously characterized charge emision from surfaces bombarded by electrospray plumes [4]. While this work thoroughly investigated charge emission with "as-received" materials commonly used in experimental facilities and spacecraft, factors such as surface roughness and contaminants — which are known to impact secondary electron emission in high energy environments — were not considered. Less experimental work has been done on analyzing the mass loss resulting from impingement of electrospray plumes in the purely ionic regime (PIR). Mass loss in experimental facilities result in free particles in a highly controlled environment that could deposit on highly sensitive diagnostics measuring thrust or current, resulting in inaccurate values for critical flight parameters. Given that low thrust electric

[1]Graduate Research Assistant, Department of Aerospace Engineering, avinash4@illinois.edu
[2]Graduate Research Assistant, Department of Aerospace Engineering, tanapat2@illinois.edu
[3]Professor, Department of Aerospace Engineering, and AIAA Associate Fellow, rovey@illinois.edu
[4]Professor, Department of Aerospace Engineering, and AIAA Fellow, deblevin@illinois.edu
[5]Associate Professor, Department of Aerospace Engineering, hbchew@illinois.edu

propulsion devices on spacecraft must be operated over extended time frames for most maneuvers, any surface erosion on surfaces downstream or adjacent to a thruster can have significant effects on the performance and lifetime of a spacecraft. Experiments are being conducted to evaluate the material interactions for typical spacecraft and experimental facility materials bombarded by an IL electrospray plume. Data on material interactions can provide more accurate methods of interpreting electrospray data collected in experimental facilities as well as potentially inform material selection and thruster design for future spacecraft missions utilizing electrospray propulsion.

Although molecular dynamics simulations are at length and time scales that are many orders of magnitude smaller than experimental setups, the ability to model emissions at these scales can assist in characterizing the behavior of an ionic liquid in the presence of an accelerating electric field. While all-atom simulations are often computationally expensive, they ensure that every atom that comprises a molecule is represented. After a system is equilibrated, properties such as the density of the bulk ionic liquid are used as a baseline to confirm that the model reflects a physical system. When an electric field is applied to bulk ionic liquid, species including monomers, dimers, and trimers are accelerated and emitted from the bulk ionic liquid over time. An accurate model of the ionic liquid in the presence of an electric field would allow for the prediction of the primary species emitted by an electrospray that may contribute to mass losses upon colliding with a metallic surface. A model would also need to capture phenomena such as Taylor Cone formation that are present in physical, experimental setups. Having a simulation would allow for the identification of the effects that adjustments to parameters such as the electric field depth have on the ionic liquid and the species emitted prior to fabricating a physical system.

II. Experimental Setup

All experiments were conducted in a 24" diameter by 27" belljar vacuum chamber. The chamber is equipped with a Leybold DB16 rough vacuum pump and a CTI Cryo Torr 8 cryopump driven by a Brooks 9600 helium compressor. The chamber is monitored by a convection enhanced Pirani gauge at low vacuum and a hot filament ion gauge at high vacuum. In this configuration, the chamber has a base pressure of 5E-6 Torr, with all experiments conducted at operating pressures of P <1E-5 Torr. The electrospray source is mounted on a Newmark Systems RM-3 rotary stage to allow for multiple diagnostics to be conducted during a given pump down cycle.

Building upon fundamental electrospray studies done previously at the University of Illinois, the ion source in these experiments is a single emitter "thruster" with an externally wetted tungsten wire emitter and a stainless steel pinhole extractor [4]. The emitters are manufactured from commercially available 0.5 mm diameter tungsten wire in accordance with the electrochemical etching process detailed in Ref. [5]. The tip of a 40 mm long section of tungsten wire is dipped in a 1N solution of NaOH and H_2O biased to 50 V. When a smooth, concave curvature to the tip is achieved, shorter dips in a 25 V solution are done until the tip is rounded. The solution is then lowered to 5 V and the needle is dipped in fully to remove the oxide layer on the needle. With the tips of the emitter etched, a 7.5 mm long section of 0.25 mm tungsten wire is then spot welded onto the needle, approximately 3 mm behind the tip. The last step of the emitter manufacturing involves microetching grooves onto the needle and crossbar to improve surface wettability. The emitter-crossbar assembly is plunged into a 4N solution of NaOH and H_2O saturated with $K_3Fe(CN)_6$ and heated to 100°C for 60 seconds. Figure 1 shows three emitters that have been fully manufactured, with the measured radius of curvature R_{tip} noted in the caption. Emitter geometry was measured optically using plain ImageJ to process the images in Fig. 1 [6].

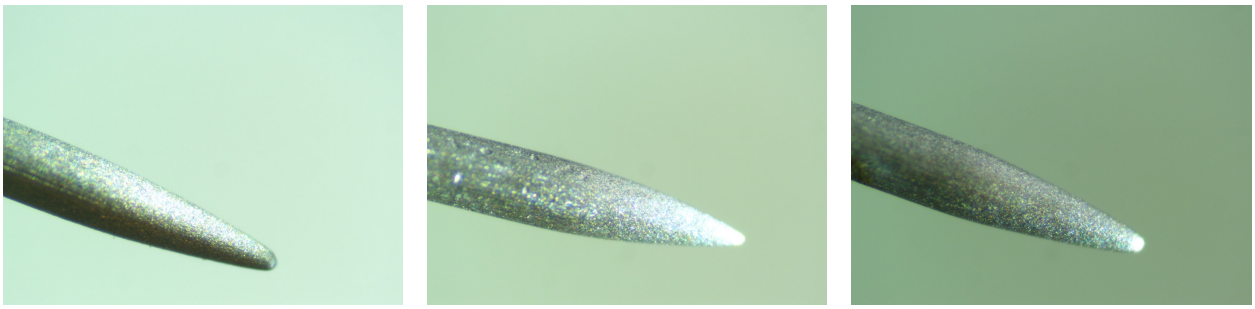

(a) R_{tip} **= 52.7** μ**m** **(b)** R_{tip} **= 42.2** μ**m** **(c)** R_{tip} **= 48.4** μ**m**

Fig. 1 Electrochemically Etched Tungsten Wire Externally Wetted Emitters

Multiple ionic liquids have been shown to be reliable as propellants in electrospray systems. For the purposes of these experiments, 1-Ethyl 3-methylimidazolium tetrafluoroborate [EMIM]-[BF_4] was chosen due to its noted ease of use in similar systems [5]. The emitter preparation and loading procedure was developed for maximum propellant wettability and propellant longevity. An etched emitter is cleaned in three ultrasonic baths: first in deionized (DI) water, then in isopropyl alcohol (IPA), and finally in acetone. After the last bath, the needle is gently rinsed with DI water and IPA again to remove any remaining residue from the acetone before being brushed off with dry air. Once dry and clean, the needle is then heated on all sides for 15 seconds with a medium temperature heat gun before a single droplet of [EMIM]-[BF_4] is dragged over the tip on all sides and then deposited onto the crossbar. The heating of the emitter improves initial wetting, while the thorough cleaning and drying ensures that no water is present for the highly hygroscopic IL to interact with. Figure 2a shows an emitter loaded with [EMIM]-[BF_4] after a full cleaning and drying. The emitter is then placed in a grooved copper electrode and clamped into the extractor assembly shown in Fig. 2b. The entire extractor assembly remains isolated from the emitter electrode by a PTFE shroud. The extractor plate is a 1 mm thick stainless steel plate with a 1.5 mm pinhole in the center. The emitter is placed in the PTFE sheath such that the tip is approximately 0.1 to 0.2 mm behind the extractor, centered on the pinhole, as shown in the top-down view in Fig. 2c.

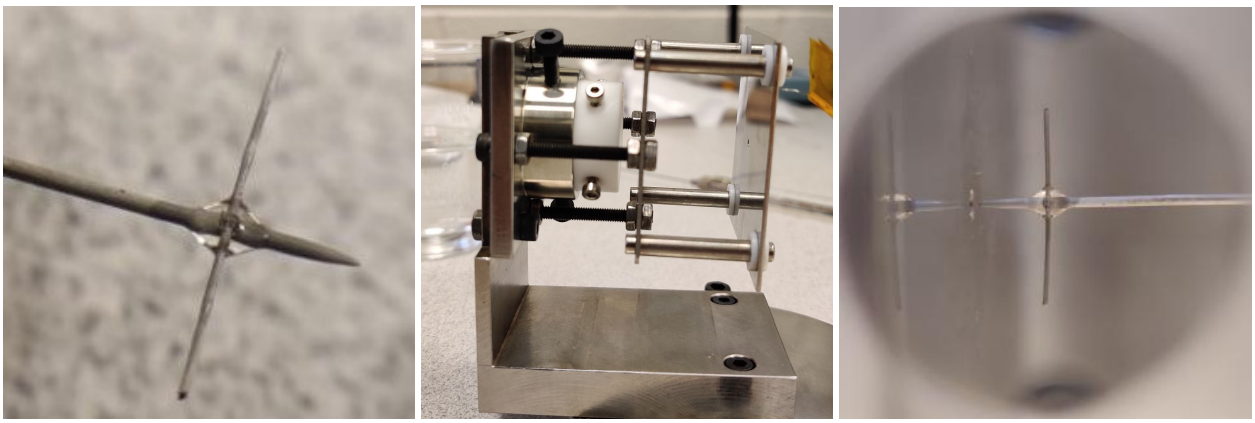

(a) Loaded Emitter **(b) Extractor Assembly** **(c) Aligned Emitter**

Fig. 2 Emitter Preparation Process

The emitter is driven by a 1 Hz square wave at a 50% duty cycle with an amplitude twice the desired emitter bias. The power source used to bias the emitter is a Matsusada AMS 5B6 high voltage amplifier. The extractor is grounded in all experiments. To reduce the likelihood of return current or secondary charged species arriving at the emitter, the entire assembly is then covered in 0.1 mm thickness kapton tape. Return current is permitted to reach the outward face of the extractor plate. A sketch of the electrical configuration of the experimental setup is shown in Fig. 3. Current output from the emitter (I_{em}) and current received at the target plate (I_{tar}) are measured by individual evaluation modules consisting of a Texas Instruments AMC1311 isolation amplifier and a 1 MΩ shunt resistor. To account for the monopolarity of the isolation amplifier, zener diodes are used to direct current based on the polarity of the emission at

any given instance. Extractor current (I_{ex}) is measured by a Keithley 6514 electrometer across a 2 MΩ shunt resistor. Additional plume diagnostics (angular distribution, energy distribution) are also conducted using a Kimball Physics Faraday cup. The current measured at the Faraday cup is collected by the Keithley electrometer. All data is passed through a National Instruments USB 6211 DAQ.

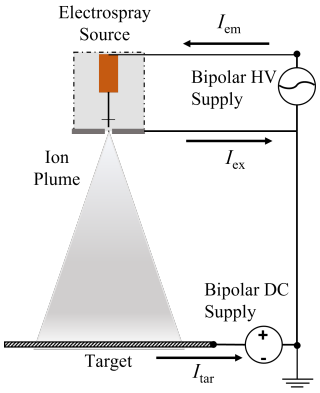

Fig. 3 Electrical Configuration of Experiment Setup

III. Modeling

An all-atom [EMIM]-[BF_4] system was implemented using the Large-scale Atomic/Molecular Massively Parallel Simulator (LAMMPS) to model the extrusion of an ionic liquid from an emitter. While the experimental setup is at length and time scales larger than can typically be captured by molecular dynamics, an atomistic model will enable the creation of a piecewise model capable of characterizing larger systems. In this simulation based on previous molecular dynamics work, 1,000 [EMIM]-[BF_4] molecules were placed in a 64 x 64 x 202.72 Å simulation domain, as shown in Fig. 4 [7]. Periodic boundary conditions were applied in the X- and Y-dimensions while the Z-dimension was fixed so that any particles that exited the domain were deleted. A Lennard-Jones 12-6 potential wall with the properties of Platinum was placed below the bulk liquid at z = -2.72 Å to attract the [EMIM]-[BF_4] molecules and contain them throughout the simulation [7]. The liquid-vacuum interface begins at approximately z = 64 Å with the vacuum extending to z = 200 Å. The system was then equilibrated for 100 picoseconds with a canonical (NVT) ensemble applied at a temperature of 298.15 K.

An electric field of 6 V/nm was applied to the system at various depths into the bulk [EMIM]-[BF_4] system with a microcanonical (NVE) ensemble for 100 ps. The electric field was placed starting at z = -2.72, 34, and 54 Å. These locations correspond to an electric field that encompasses the entire bulk ionic liquid, half of the bulk ionic liquid, and a region starting at 8 Å below the liquid-vacuum interface, respectively. The field of 6 V/nm was then applied to the entire bulk ionic liquid for 100, 200, and 1,000 ps. In addition to the applied electric field, a moving potential wall was considered to model the extrusion of ionic liquid from an emitter. The appropriate wall velocity can be obtained from a mass flow rate. In one experiment, EMIM-BF4 was extruded from an emitter with a 10-micron radius at an inferred mass flow rate of 0.561926e-12 kg/s [8]. This corresponds to a moving wall velocity of about 1.4e-8 Å /ps. As a result, it can be concluded that the movement of the wall is negligible within the molecular dynamics timescale, and the Lennard-Jones wall remained fixed for the entire simulation. In this simulation, emissions from the bulk ionic liquid are due to the electric field. Counts of the emitted species were tracked for all cases.

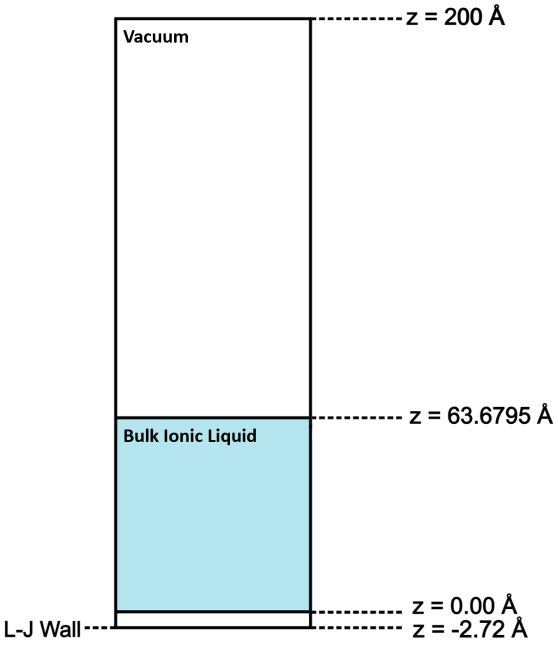

Fig. 4 Simulation Domain Setup for 1,000 Ionic Liquid Molecules

After the ionic liquid was equilibrated for 100 ps, the average density of the bulk ionic liquid over time was computed by excluding bins closest to the surface and the Lennard-Jones potential wall. The final average density of the bulk ionic liquid was found to be 1.252 g/cm^3, which is in good agreement with the densities observed empirically [9–11].

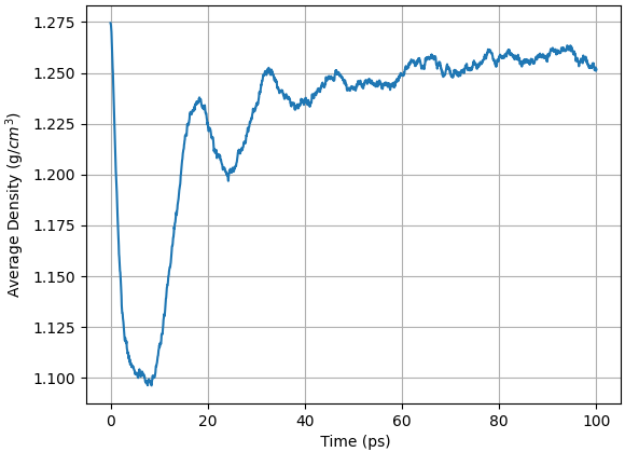

Fig. 5 Average Density of Ionic Liquid Over Equilibration Time [12]

With the ionic liquid in an equilibrated state, the placement of the electric field and simulation runtime were varied. Varying the depth of the electric field was done to visualize the formation of an electric double layer as was seen in previous work [7]. While there were not enough emissions within 100 ps to determine the effects of the electric double layer on emissions, it was observed that the double layer formed at the depth where the electric field was placed. In Fig. 6, only boron atoms in the ionic liquid are displayed along with a line indicating where the electric field was applied. This was done to clearly visualize the double layer that forms around each line. When varying the simulation runtime, the 6 V/nm electric field was applied to the entire domain (z = -2.72 to 200 Å) as this best represents the experimental setup. Since the electric field is implemented instantaneously in all cases, the atoms in the bulk ionic liquid accelerate as they adapt to the introduction of the field. The initial burst of emissions that occurs while the system is still transient is not included in the counts of emitted species over time.

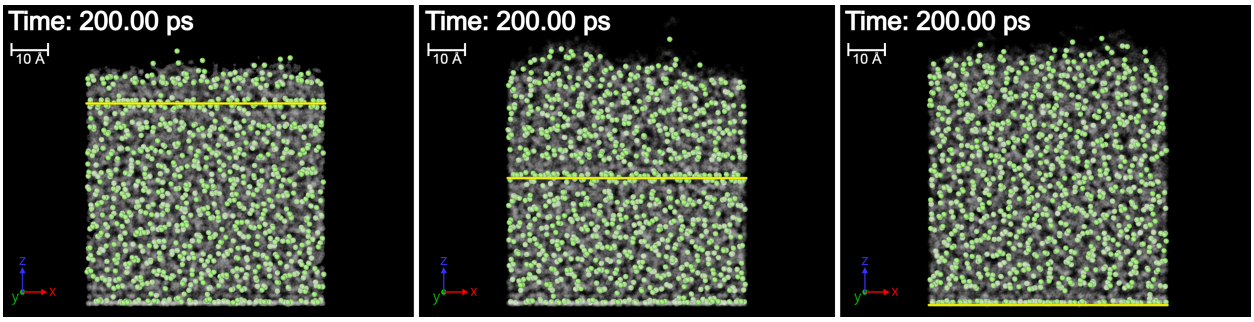

Fig. 6 Boron Isolated from Anions in the Bulk Ionic Liquid: z = 54 Å (Left), z = 34 Å (Center), and z = -2.72 Å (Right) [12, 13]

When the electric field was applied at z = 54 Å, there were 3 [EMI^+] cations and 3 [EMIM-BF_4]-[EMI] dimers emitted between 114.75 and 138.70 ps. The second dimer emitted at 123.90 ps fragmented into a monomer and a [EMIM]-[BF_4] neutral pair at 126.05 ps. At z = 34 Å, there were 6 cations emitted between 114.10 ps and 195.90 ps. When the electric field was applied to the entire domain, there was 1 cation and 1 dimer between 155.30 ps and 175.45 ps. While there were fewer emissions when the electric field was applied to the entire domain, there were not enough emissions over time to attribute this observed decrease to the electric double layer formation. Since the double layer forms where the electric field is applied, it is possible that this a nonphysical artifact of the numerical simulation indicative of a region where the electric field strength decreases abruptly to 0 V/nm.

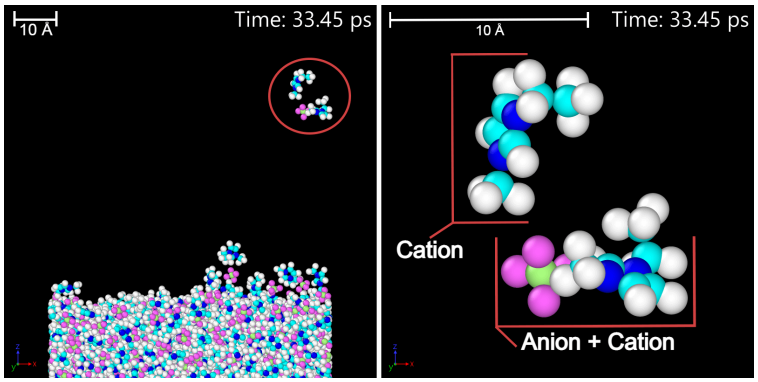

Fig. 7 Fragmentation of First Dimer Emitted from Bulk Ionic Liquid for 1,000 ps Simulation (Left) with Zoom of Circled Fragment (Right) [12, 13]

When the 6 V/nm electric field was applied for 100 ps, there were two emissions. For the 200 ps run, there were four emissions. In both of cases, only cations and dimers were emitted. Over 1,000 ps, there were 13 emissions including [EMIM-BF_4]$_2$[EMI^+] trimers and a neutral pair of [EMIM-BF_4]. The first dimer emitted at 32 ps fragments into a cation and a neutral pair (see Fig. 7). The neutral pair then fragments into a cation and an anion. While doubling the simulation time from 100 ps to 200 ps led to doubled the number of emissions, a fivefold increase from a 200 ps to 1,000 ps did not lead to a similar increase in the number of particular species emitted. Instead, additional species such as trimers were detected while the overall count of emitted species increased by a factor of 3.25. The emitted species are compiled in Table 1.

Table 1 Emissions from Bulk Ionic Liquid for Varied Simulation Times

Time, ps	Cations	Dimers	Trimers	Neutral Pairs
100	1	1	0	0
200	2	2	0	0
1000	4	6	2	1

In the 100 ps simulation, a Taylor Cone does not form; however, for the 200 and 1,000 ps simulation, a Taylor Cone starts to form at around 165 ps. As shown in Fig. 8, a clearly defined Taylor Cone forms in the 1,000 ps simulation at 404.45 ps. The limited number of emitted species and lack of a well-defined Taylor Cone at 100 and 200 ps indicates that the system may not have had a sufficient time to reach steady state after the introduction of the electric field. This contrasts with the 1,000 ps simulation where a Taylor Cone forms and species are emitted. The Taylor Cone collapses and reforms over the run as the ionic liquid interacts with the electric field. The presence of the Taylor Cone indicates that complex phenomena observed on larger, experimental scales can be observed in the atomistic model. Further analysis of this setup will be required to provide insights into the factors that contribute to Taylor Cone formation.

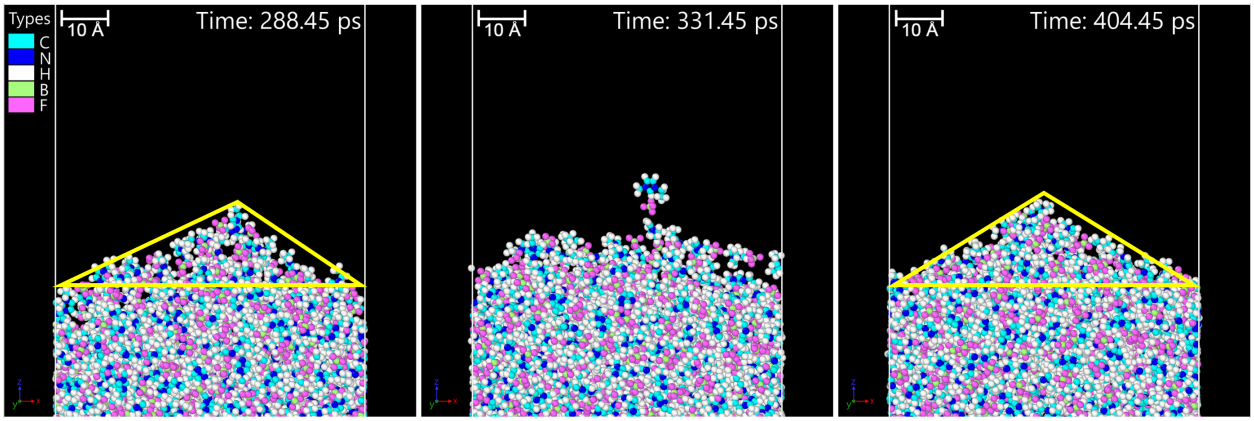

Fig. 8 Taylor Cone Forming (Left), Taylor Cone Collapsing (Center), Taylor Cone with 61.6° Half-Angle (Right) for 1,000 ps Simulation [12, 13]

In order to obtain a sufficient number of emissions for further analysis, the simulation will need to be accelerated. This will involve increasing the simulation time, changing the temperature of the system, and running several optimized scenarios in parallel. Increasing the simulation time will allow the system more time to produce emissions after reaching a steady state while changing the temperature may lead to changes in the number of emitted species overall. Once the atomistic model is validated, a piecewise model comprised of several atomistic simulations at representative locations of a larger-scale system can be developed to capture the behavior of an experimental setup.

IV. Experimental Results

A. Emitter Operation

In order to accurately represent the interactions between the electrospray plume and the material surfaces, both elements must be characterized thoroughly. Figure 9 displays three diagnostics conducted. Figure 9a shows anion I-V curves for three different emitters. The same extractor pinhole was used in all cases. Figure 9b displays anion and cation I-V curves for a single emitter and extractor. These I-V curves were collected with no target directly downstream of the electrospray source and the nearest downstream surface was the chamber wall 60 cm away from the plane of the extractor plate. At this distance, it can be assumed that return current from secondary charge emission is low enough to be negligible, as demonstrated by Klosterman *et al.* [4]. Over the range of applied emitter biases, the extractor current remained between 5% and 8%. Figure 9c represents the angular distribution of the electrospray plume for three emitters. This normalized current measurement was captured by sweeping the electrospray source while measuring received current with a Faraday cup held 5 cm in front of the extractor plane. Note that the plume half-angle ranged from 15° to 23° for the three emitters that were studied. The slight variability in emitted current and angular distribution likely arises from the minute variance in curvature of the tip of the emitter, as shown in Fig. 1.

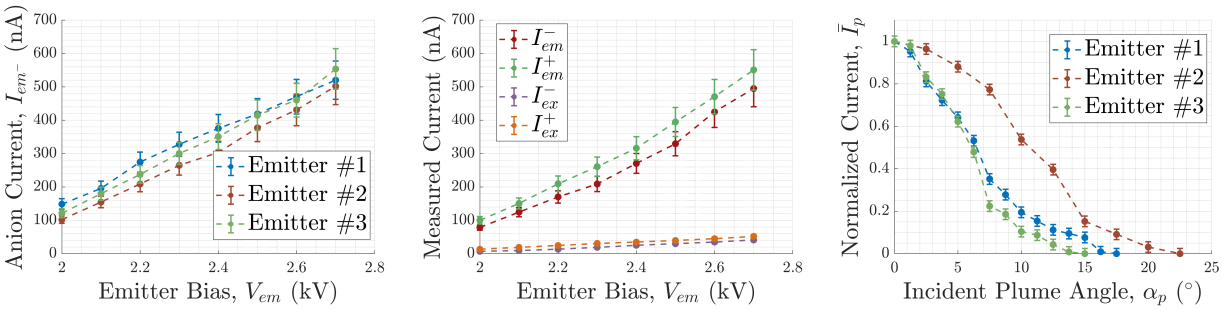

(a) Anion IV Curves **(b) Emitter and Extractor Current** **(c) Plume Half-Angle Distribution**

Fig. 9 Initial Diagnostics Conducted on Electrospray Plume

B. Bombardment Target Preparation

Previous works investigating secondary electron emission and ion-induced electron emission have noted that surface roughness can impact ion induced electron emission yields. Models of plasma interactions with rough metallic surfaces observed that yields generally decreased with surface roughness, as emitted secondaries could become trapped in elevated surface features [14]. Although previous work at the University of Illinois investigated ion-induced charge emission for different materials, surface trapping effects were not accounted for directly. To control for surface roughness, all materials samples were polished to a mirror finish. Mirror finish is generally accepted as the surface quality in materials surface studies wherein surface features can be ignored, qualified by a root-mean square roughness $S_q \in [30, 160]$ nm [15]. In order to achieve this level of surface finish, as-received samples of aluminum 6061 and 316 stainless steel were processed in a GIGA1200 Vibratory Polisher. Both specimens are 15 cm x 15 cm square plates, large enough such that they capture the full emitted plume when placed 8 cm downstream of the extractor. After processing, each of the materials was optically profiled using a Keyence VK-X1000 3D Laser Confocal Microscope. Ten randomly sampled areas over the surface of each material were scanned in laser confocal mode at fifty times magnification. The S_q was calculated for each area and the average was calculated for each material, as tabulated in Table 2. Comparisons of an area on each of the samples are shown in Fig. 10.

Table 2 Surface Roughness of Materials Measured by Keyence VK-X1000 with Accuracy of 0.5 nm

Material	Unfinished S_q (nm)	Pre-polished S_q (nm)	Polished S_q (nm)
Aluminum 6061	521	651	161
316 Stainless Steel	283	256	106

(a) Al6061 Pre-polishing **(b) Al6061 Post-polishing** **(c) 316SS Pre-polishing** **(d) 316SS Post-polishing**

Fig. 10 Surfaces of Bombardment Targets Before and After Polishing, Measured via Laser Confocal Microscopy, Magnified to 50x

The polished sample was the main test article in the secondary charged species emission experiments detailed herein. Identical experiments were conducted on similar unfinished, as-received samples which were used in experiments

previously conducted at the University of Illinois [4]. These as-received samples were used as a control specimen, so data could be compared with previously established results.

Initial results from prior experiments also did not account for the presence of hydrocarbon contaminants and their potential impact on secondary charge yields. Surface compositions of bombardment targets were characterized on as-received samples via X-ray photoelectron spectroscopy (XPS) and time-of-flight secondary ion mass spectroscopy (ToF-SIMS) in Klosterman *et al.*, and showed significant concentrations of C and O_2 atoms on the topmost surface layers of the bombarded targets [4]. To attempt to eliminate this layer of hydrocarbon contaminants, the polished material samples were also baked in vacuum. Baking vacuum facilities is a common practice in high and ultra high vacuum systems where partial pressures of adsorbed volatiles can deteriorate vacuum quality and interfere with measurements. For the purposes of these experiments, the vacuum bakeout was intended to remove any of these adsorbed volatiles from the surface of the material so the incident $[EMIM]^+$ and $[BF_4]^-$ ions impact and interact with metal and metal oxide atoms rather than hydrocarbon contaminants. Experiments conducted by Goh *et al.* at the University of Michigan investigated contamination of stainless steel and aluminum in transmission electron microscopy (TEM) hardware and cited a decrease in water vapor and common organic species by four orders of magnitude after baking at a temperature of 130°C for 48 hours [16]; note that the low baking temperature was set by the low temperature requirements of sealing hardware used in TEM setups. Given that no such sensitive hardware is present on the polished target, and ref. [17] specifies that higher baking temperatures up to 300° result in improved post-baking partial pressures at lower baking times, the polished sample was baked at 200°C for only 8 hours and allowed to return to room temperature before conducting charge emission experiments. Figure 11 shows the reverse side of the polished bombardment target with the mounting hardware, patch heater and thermocouple affixed. The patch heater is an Omega PLM-304/10 polyimide heating element, and the bakeout was controlled using and Omega CN730 temperature controller monitored by a K-type thermocouple. All pieces were mounted onto the reverse face of the target using polyimide Kapton tape with a high-temperature silicone adhesive.

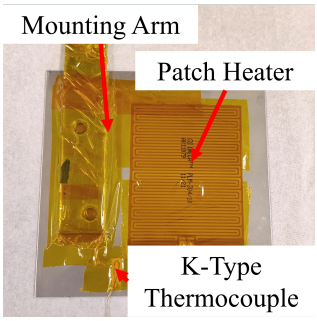

Fig. 11 Bakeout Setup on Polished Sample

C. Charge Emission from Biased Targets

Secondary charge emission was studied by varying the bias on the bombardment target, resulting in enhancement and suppression of yields as a function of the surface bias. Studies conducted at the University of Southampton and UCLA as well previous work at the University of Illinois have investigated electrostatic suppression of secondary charge yield, whether using biased targets or charged grids [4, 18, 19]. For the purposes of these experiments, biasing the targets themselves was selected as the mode of suppression/enhancement, as a suppression grid introduces another surface off of which secondaries can be emitted and obscure the true yield from the target material. The general trend expected in biased target studies would be an increased yield of secondary negative and a decreased yield of positive species when the target is biased negatively. Emitted negative species with lower secondary energy are repelled by the negative target bias, while positive secondaries with low enough energies are attracted back to the negatively charged surface. Using the same logic, it is to be expected that a positively biased target would have a lower yield of secondary negatively charged species and an enhanced yield of secondary positively charged species.

To observe these trends, the electrospray plume was directed at a target while the target was swept from a low negative voltage to a low positive voltage. The electrospray source was oriented such that the centerline of the emitted plume was parallel to the target normal in all cases. The maximum target bias must be low enough such the resultant

field strength was insignificant compared to the energy of even the lowest energy primary ions. Therefore, the target sweep was conducted from -30 V to 30V at 5 V increments, with the target bias being held for 5 s at each incremental voltage. One 5 second increment during a test with polished Al6061 is shown in Fig. 12. As mentioned previously, the emitter was operated in a 1 Hz square wave in order to deliver both cation and anion currents to the target. This mode of operation also prevented charge buildup on the emitter or target and deters electrochemical fouling at the emitter tip. Note the onset overshoot in currents coinciding with the change in polarity in each square wave pulse. Similar behavior has been noted in comparable externally wetted systems and characterized in work completed by Lozano and Martinez-Sanchez [5].

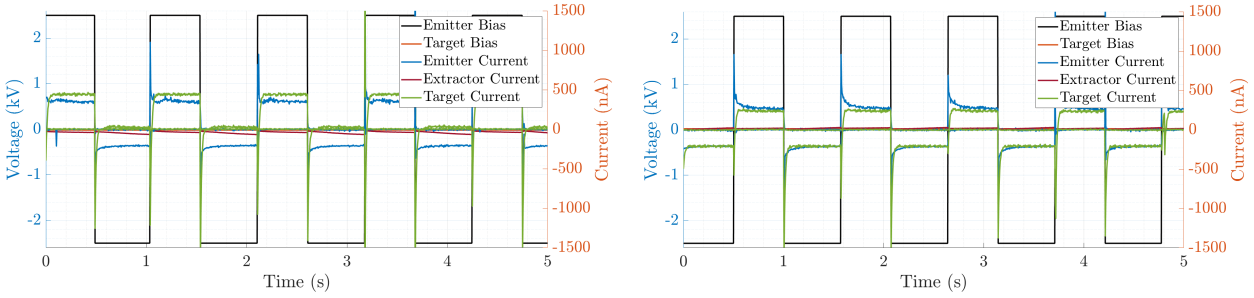

(a) $V_{\mathbf{tar}} = -20$ **V** **(b)** $V_{\mathbf{tar}} = +20$ **V**

Fig. 12 Raw Current Traces Collected During Target Bias Sweep

The measured current at the target was higher than the sum of emitter and extractor currents in Fig. 12a, when the target voltage was -20 V; conversely, Fig. 12b shows the measured target current being lower than the sum of emitter and extractor currents when the target was biased up to +20 V . These discrepancies are evidence of different types of secondary charge emission. The average currents are calculated for each polarity over the 5 s span at each target bias. The aforementioned onset overshoot was disregarded from each average. After taking the averages, the currents can be displayed as a function of the target bias sweep, as in Fig. 13.

Similar trends in the averaged current traces were present in all cases, regardless of surface material or quality. Focusing first on the case with the unfinished aluminum sample as shown in Fig. 13a, changes in the target, emitter, and extractor current correlate to the bias on the bombardment target. The target current during cation bombardment decreases from 375 nA to 200 nA as the target bias sweeps from -27 V to 23 V. The emission of cations appeared to change as the target bias sweeps. Initially, 325 nA of cation current was emitted when the target was floated to -27 V, increasing to 375 nA when the target was held at 0V, and decreasing down to 345 nA when the target reached 23 V. Conversely, the anion current emission remained a constant -200 nA throughout the target bias sweep, while the measured target current dropped from 25 nA to -200 nA as the target bias was swept. Current collected at the extractor seemed to follow similar trends in both modes of operation. Whether cations or anions were impinging on the extractor, -80 nA of extractor current were measured when the target was biased negatively. As the target bias became more positive, the extractor measured 40 nA of current when antions were being emitted, and 50 nA when cations were being emitted. The amount of extractor current noted in these experiments was much higher than the 5%-8% of impingement current measured in initial diagnostics without a bombardment target downstream. This excess in extractor current can be attributed to the portion of secondary charged species returning to the grounded extractor.

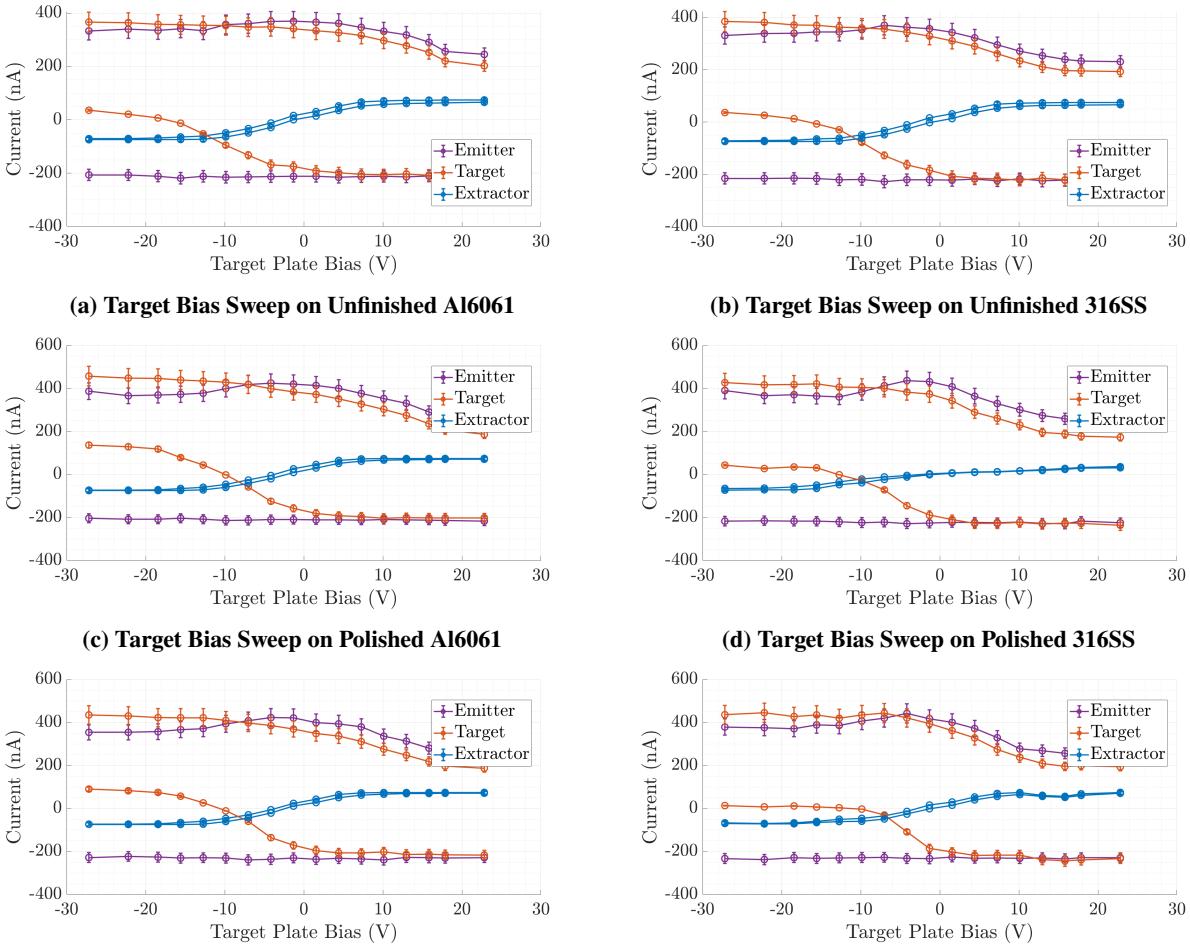

(a) Target Bias Sweep on Unfinished Al6061

(b) Target Bias Sweep on Unfinished 316SS

(c) Target Bias Sweep on Polished Al6061

(d) Target Bias Sweep on Polished 316SS

(e) Target Bias Sweep on Polished and Baked Al6061

(f) Target Bias Sweep on Polished and Baked 316SS

Fig. 13 Current Traces for Material Samples with Different Surface Finishes and Qualities at an Emitter Voltage of V_{em} = 2.5 kV

V. Analysis and Discussion

In order to accurately describe the secondary charge emission yield, the measured currents must be translated to currents of secondary and primary charged species. As noted previously, a portion of the emitted current impinges on the upstream face of the extractor. Therefore, the plume current can be expressed as a difference of the current measured leaving the emitter I_{em} and the current arriving at the extractor I_{ex}. However, when a surface was placed downstream of the extractor, secondary currents can return to the downstream face of the extractor face and contribute to the measured extractor current. As such, the extractor current measured with no surfaces immediately downstream — defined as $I_{ex,0}$ — was used to calculate the plume current, as expressed in Eq. (1). The measured target current encapsulates both the primary ions striking the specimen, as well as the charge deficit resulting from charged particles leaving the surface. Therefore, the secondary current can be expressed as a simple difference between the plume current I_{plume} and the measured target current I_{tar}, as in Eq. (2).

$$I_{plume} = I_{em} - I_{ex,0} \tag{1}$$

$$I_{sec} = I_{plume} - I_{tar} \tag{2}$$

These derived current values can then be used to express the yields of secondary charged species per incident

primary ions, $\gamma \left[\frac{\text{charge}}{\text{ion}}\right]$. From the average current traces in Fig. 13, four distinct yields can be identified. When positive cations strike the surface of a positively biased target, the target current was lower than the plume current, indicating an emission of positive charges from the target surface. This cation induced positive charge yield value, γ_+^+ was calculated as in Eq. (3). When cations struck a negatively biased surface, the higher target current indicated emission of negative charges, so a cation induced negative charge yield γ_-^+ could be calculated using Eq. (4). For the case of anions bombarding a positively charged surface, a positive secondary charge emission resulted in an anion induced positive charge yield γ_+^- as expressed in Eq. (5). Lastly, anions striking a negatively biased surface resulted in an emission of negative charges, such that Eq. (6) could describe an anion induced negative charge yield γ_-^-.

$$\gamma_+^+ = \frac{\left|I_{\text{sec,cat}}^+\right|}{\left|I_{\text{plume,cat}}\right|} \tag{3}$$

$$\gamma_-^+ = \frac{\left|I_{\text{sec,cat}}^-\right|}{\left|I_{\text{plume,cat}}\right|} \tag{4}$$

$$\gamma_+^- = \frac{\left|I_{\text{sec,an}}^+\right|}{\left|I_{\text{plume,an}}\right|} \tag{5}$$

$$\gamma_-^- = \frac{\left|I_{\text{sec,an}}^-\right|}{\left|I_{\text{plume,an}}\right|} \tag{6}$$

$$\tag{7}$$

The main investigation undertaken was to explore whether or not the secondary charged species yield have any dependence on the surface finish or baking. In addition, the yields from the different surface qualities were compared to previous work from Klosterman *et al.*, where as-received specimens for a variety of materials were tested to study ion-induced charge emission from different target materials [4]. This data is denoted by "UIUC, 2021" in Figures 14 and 15, where the four different secondary charge yields for aluminum 6061 and 316 stainless steel are compared.

Note that in all cases, there does not seem to be any clear and consistent correlation between the material's surface finish and the secondary charge yield. Focusing on Figures 14c and 15c, the anion induced positive charge yields are all so low so as to be attributable to signal noise. Conversely, the anion induced negative charge yields as shown in Figures 14d and 15d are all much higher, with most variance falling within the 10% error resulting from measurement uncertainty in the isolation amplifiers used to measure low currents at high floating voltages. More confounding are the cation induced yields. Figure 14a shows that the data previously collected by Klosterman *et al.* on aluminum 6061 agrees well with the yields from the polished surface, while the unfinished surface has higher yields that match well with the baked and polished surface. For stainless steel, Fig. 15a shows that the cation induced positive yields for the polished surface agree with the yields from the polished and baked surface, indicating that the hydrocarbon content had little impact on this specific yield. However, the yields from the unfinished surface do not match the yields from the as-received stainless steel studied by Klosterman *et al.* The cation induced negative charge yields from the aluminum surfaces tested show good agreement with each other aside from the yields measured by Klosterman *et al.*, which are all 2-5x higher than those measured in these experiments, and increase with emitter voltage rather than decrease. Comparatively, the cation induced negative charge yields shown in Fig. 15b match better for the stainless steel surfaces, but still exhibit enough variation that can neither be easily attributed to measurement uncertainty, nor be logically explained by differences in surface quality. The yields measured by Klosterman *et al.* were generally higher than those measured in these experiments, where the polished and baked surface showed a slightly higher yield than the unfinished surface and the polished surface, which exhibited yields that agree well with each other.

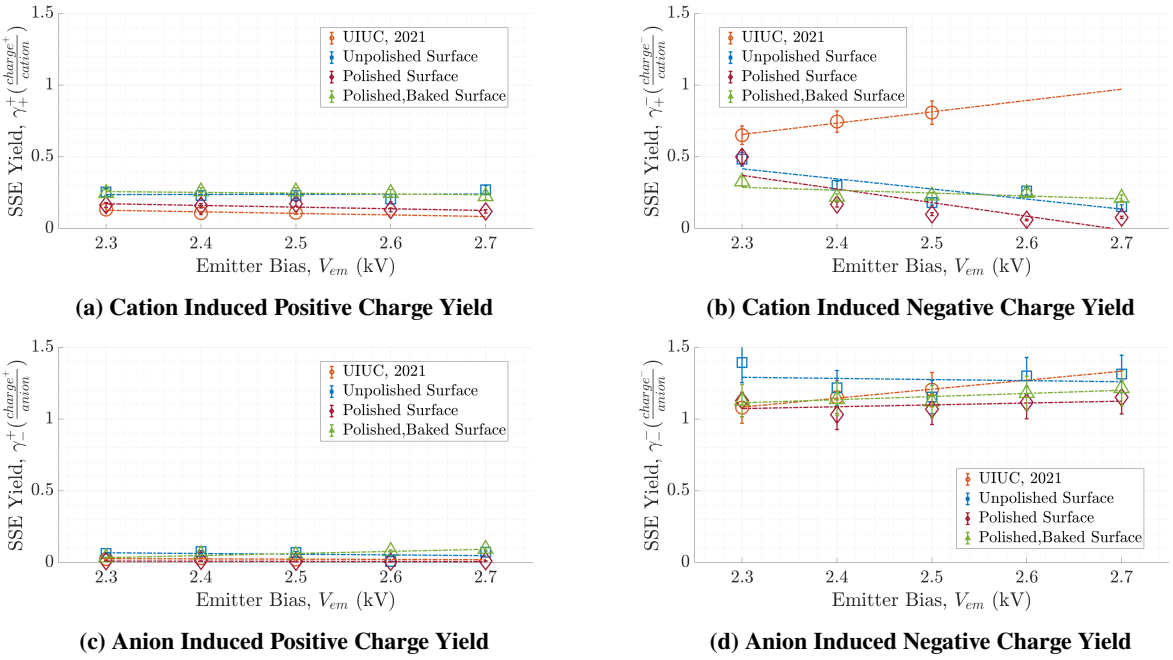

(a) Cation Induced Positive Charge Yield

(b) Cation Induced Negative Charge Yield

(c) Anion Induced Positive Charge Yield

(d) Anion Induced Negative Charge Yield

Fig. 14 Aluminum Yields Compared with Previously Collected Data at UIUC

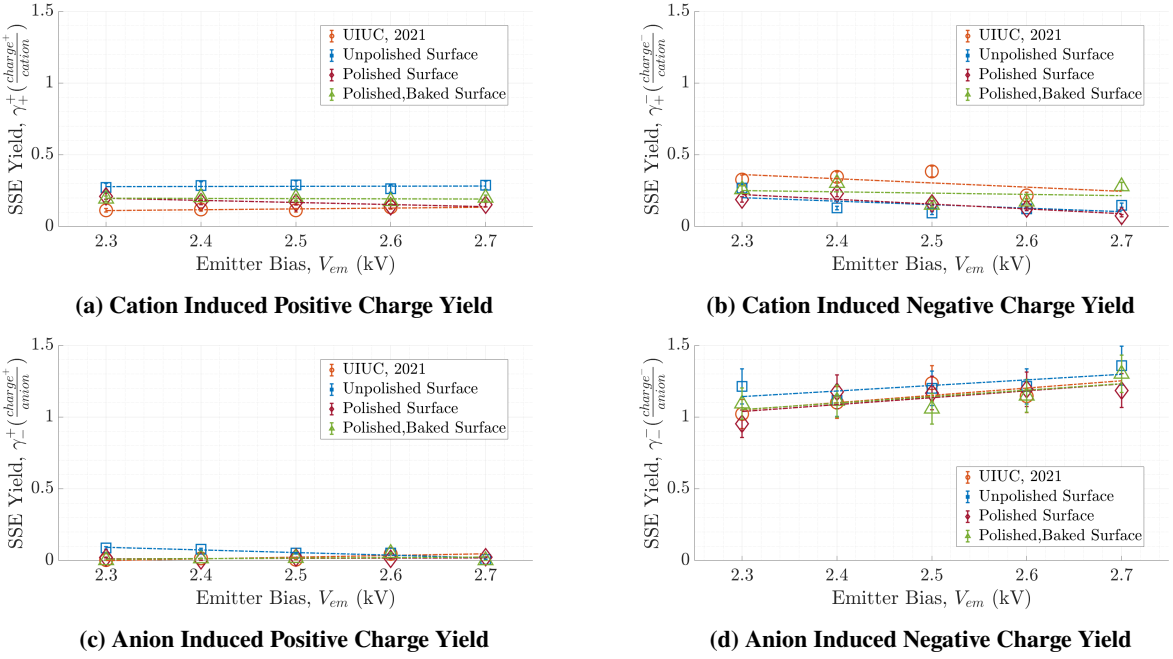

(a) Cation Induced Positive Charge Yield

(b) Cation Induced Negative Charge Yield

(c) Anion Induced Positive Charge Yield

(d) Anion Induced Negative Charge Yield

Fig. 15 Stainless Steel Yields Compared with Previously Collected Data at UIUC

From these results, no clear conclusions can be drawn regarding the impacts of low surface roughness or vacuum baking on secondary charged species emission from aluminum and stainless steel surfaces. What can be concluded is that a number of factors not controlled for in previous secondary charge experiments with electrosprayed polyatomic ions. One notable difference that could contribute to the difference in measured yields was the amount of current output by the different electrospray sources. The plume current measured in the experiments conducted by Klosterman *et al.* were on the order of 800-1000 nA, whereas the currents measured here ranged from 300-500 nA. Although yield is a

parameter normalized by incident current, and as such should not be directly influenced by the number of incident ions, the density of the plume could impact measured current values, as collisions between primaries and emitted secondaries could decrease the energy of ions prior to impact with the target ions, reducing the likelihood of secondary emission. No thorough studies of 3D plume distribution have been conducted in these experiments. This consideration also leads to the question of how representative yields resulting from a single emitter are in respect to full electrospray thrusters. Electrospray thrusters are commonly arrayed to improve performance, resulting in hundreds of emission sites emitting hundreds of times more current than a single emitter. To study these realistic effects, similar studies as to the ones conducted here will be conducted using a porous glass thruster based on the AFET-2 design [20]. The thruster is being manufactured by the Electric Propulsion Lab at the University of Illinois Urbana-Champaign using novel manufacturing methods.

Furthermore, angle-of-incidence is known to impact ion-induced charge emission, as established by experiments conducted by Svensson *et al.* [21]. In these experiments and the experiments conducted by Klosterman *et al.*, the plume impinging upon the bombardment target contains primary ions with relative incidence angles ranging from 0° to 23°. To account for this potential confounding factor, a unidirectional beam can be produced by the same electrospray source used in these experiments by adding an Einzel lens downstream of the thruster. An Einzel lens, like the one designed by Lozano to study the mass-to-charge ratios of electrospray plumes, electrostatically collimates the disperse plume by generating a strong field that eliminates nonaxial velocity components of all ions within the plume [22]. The "plume" bombarding the target would then be composed of unidirectional, if not monoenergetic, ions focused on a smaller area of the target surface, removing any uncertainty introduced by varied angles of incidence.

VI. Conclusion

Secondary charged species yields were determined for three different surface finishes of aluminum 6061 and 316 stainless steel bombarded by electrospray plumes with emitter voltages of 2.3 to 2.7 kV. The materials were polished down to mirror finish, and a bakeout procedure was used to eliminate a majority of adsorbed hydrocarbons from the surface of the materials. Ultimately, no significant effect was noted due to the surface finish nor the baking. Potential causes of the variance between experimental yield values could be attributed to properties within the plume that are not controlled for. The angular distribution and energetic distribution of the primaries composing the plume are broad enough such that measuring a yield with a disperse plume does not fully capture the effects of the ion-surface interactions. Future experimental work will utilize electrostatic collimation to reduce the divergence of the beam and eliminate any effects due to varying angles of incidence. In addition, the low amount of plume current produced by the externally wetted tungsten wire emitter — while beneficial for fundamental plume studies — does not provide the most representative plume to predict behavior in electrospray thrusters. Development of a porous glass electrospray thruster based on the AFET-2 design is underway to produce a consistent plume of $[EMIM]^+$ and $[BF_4]^-$ ions with current density and magnitudes comparable to state-of-the-art electrospray systems.

The initial molecular dynamics simulations demonstrate that phenomena observed on larger scales are identifiable in these smaller scale simulations. Additionally, it was observed that as the 6 V/nm electric field interacted with ionic liquid, an electric double layer formed at the location where the field was applied over time. In order to obtain a sufficient population of emissions from the bulk ionic liquid to draw further conclusions about the impact of the electric field on the species emitted and the bulk ionic liquid, the simulation would need to be accelerated by adjusting parameters like the temperature of the system or by running for longer periods of time. As a goal of these simulations was to eventually model larger-scale experimental setups through molecular dynamics or with particle-in-cell methods, a piecewise simulation of the ionic liquid with varied electric field strengths applied to representative portions of a larger system would allow for more direct comparisons to be made at the molecular dynamics scale.

Acknowledgements

The authors thank the NASA Early Stage Innovation program, federal award identification number 80NSSC19K0215, for funding the experimental work for this project and Dr. Thomas Liu at NASA Glenn Research Center for his contributions as an advisor for the project.

References

[1] Thuppul, A., Wright, P. L., Collins, A. L., Ziemer, J. K., and Wirz, R. E., "Lifetime considerations for electrospray thrusters," *Aerospace*, Vol. 7, No. 8, 2020, pp. 1–18. https://doi.org/10.3390/AEROSPACE7080108.

[2] Mier-Hicks, F., and Lozano, P., "Spacecraft-Charging Characteristics Induced by the Operation of Electrospray Thrusters," *Journal of Propulsion and Power*, Vol. 33, No. 2, 2017, pp. 456–467. https://doi.org/10.2514/1.B36292.

[3] Magnusson, J. M., Collins, A. L., and Wirz, R. E., "Polyatomic ion-induced electron emission (Iiee) in electrospray thrusters," *Aerospace*, Vol. 7, No. 11, 2020, pp. 1–21. https://doi.org/10.3390/aerospace7110153.

[4] Klosterman, M. R., Rovey, J. L., Levin, D. A., and Rao, A., "Ion-induced charge emission from unpolished surfaces bombarded by an [Emim][BF4] electrospray plume," *Journal of Applied Physics*, Vol. 131, No. 24, 2022. https://doi.org/10.1063/5.0060615.

[5] Lozano, P., and Martínez-Sánchez, M., "Ionic liquid ion sources: Characterization of externally wetted emitters," *Journal of Colloid and Interface Science*, Vol. 282, No. 2, 2005, pp. 415–421. https://doi.org/10.1016/j.jcis.2004.08.132.

[6] Schneider, C. A., Rasband, W. S., and Eliceiri, K. W., "NIH Image to ImageJ: 25 years of image analysis," *Nature Methods*, Vol. 9, No. 7, 2012, pp. 671–675. https://doi.org/10.1038/nmeth.2089, URL https://doi.org/10.1038/nmeth.2089.

[7] Azevedo, V. A., "Molecular dynamics simulations of EMIM - BF4 ionic liquid for electrospray thrusters," Master's thesis, University of Illinois Urbana-Champaign, 2021. URL https://hdl.handle.net/2142/113004.

[8] Romero-Sanz, I., Bocanegra, R., Fernandez de la Mora, J., and Gamero-Castaño, M., "Source of heavy molecular ions based on Taylor cones of ionic liquids operating in the pure ion evaporation regime," *Journal of Applied Physics*, Vol. 94, No. 5, 2003, pp. 3599–3605. https://doi.org/10.1063/1.1598281, URL https://doi.org/10.1063/1.1598281.

[9] Nuwal, N., Azevedo, V. A., Klosterman, M. R., Budaraju, S., Levin, D. A., and Rovey, J. L., "Multiscale modeling of fragmentation in an electrospray plume," *Journal of Applied Physics*, Vol. 130, No. 18, 2021, p. 184903. https://doi.org/10.1063/5.0064711, URL https://doi.org/10.1063/5.0064711.

[10] Fan, X.-H., Chen, Y.-P., and Su, C.-S., "Density and Viscosity Measurements for Binary Mixtures of 1-Ethyl-3-methylimidazolium Tetrafluoroborate ([Emim][BF4]) with Dimethylacetamide, Dimethylformamide, and Dimethyl Sulfoxide," *Journal of Chemical & Engineering Data*, Vol. 61, No. 2, 2016, pp. 920–927. https://doi.org/10.1021/acs.jced.5b00753, URL https://doi.org/10.1021/acs.jced.5b00753.

[11] Docampo-Álvarez, B., Gómez-González, V., Méndez-Morales, T., Rodríguez, J. R., López-Lago, E., Cabeza, O., Gallego, L. J., and Varela, L. M., "Molecular dynamics simulations of mixtures of protic and aprotic ionic liquids," *Phys. Chem. Chem. Phys.*, Vol. 18, 2016, pp. 23932–23943. https://doi.org/10.1039/C6CP03700C, URL http://dx.doi.org/10.1039/C6CP03700C.

[12] Thompson, A. P., Aktulga, H. M., Berger, R., Bolintineanu, D. S., Brown, W. M., Crozier, P. S., in 't Veld, P. J., Kohlmeyer, A., Moore, S. G., Nguyen, T. D., Shan, R., Stevens, M. J., Tranchida, J., Trott, C., and Plimpton, S. J., "LAMMPS - a flexible simulation tool for particle-based materials modeling at the atomic, meso, and continuum scales," *Comp. Phys. Comm.*, Vol. 271, 2022, p. 108171. https://doi.org/10.1016/j.cpc.2021.108171.

[13] Stukowski, A., "Visualization and analysis of atomistic simulation data with OVITO-the Open Visualization Tool," *MODELLING AND SIMULATION IN MATERIALS SCIENCE AND ENGINEERING*, Vol. 18, No. 1, 2010. https://doi.org/{10.1088/0965-0393/18/1/015012}.

[14] Buschhaus, R., Prenzel, M., and Von Keudell, A., "Ion-induced secondary electron emission of oxidized nickel and copper studied in beam experiments," *Plasma Sources Science and Technology*, Vol. 31, No. 2, 2022. https://doi.org/10.1088/1361-6595/ac4c4c.

[15] Fu, S., Cheng, F., and Tjahjowidodo, T., "Surface Topography Measurement of Mirror-Finished Surfaces Using Fringe-Patterned Illumination," *Metals*, Vol. 10, No. 69, 2020, p. 11. https://doi.org/10.3390/met10010069.

[16] Goh, Y. M., Schwartz, J., Rennich, E., Ma, T., Kerns, B., and Hovden, R., "Contamination of TEM Holders Quantified and Mitigated with the Open-Hardware, High-Vacuum Bakeout System," *Microscopy and Microanalysis*, Vol. 26, No. 5, 2020, pp. 906–912. https://doi.org/10.1017/S1431927620001762.

[17] "Vacuum Physics and Technology," *Methods in Experimental Physics*, Vol. 14, edited by G. Weissler and R. Carlson, Academic Press, 1979, Chap. 14, pp. 491–503.

[18] Ma, C., and Ryan, C. N., "The Design and Characterization of a Porous-emitter Electrospray Thruster (PET-100) for Interplanetary CubeSats (CHARTS)," *Proceeding of the 7th Interplanetary CubeSat Workshop*, 2018, pp. 1–9.

[19] Uchizono, N. M., Collins, A. L., Marrese-Reading, C., Arestie, S. M., Ziemer, J. K., and Wirz, R. E., "The role of secondary species emission in vacuum facility effects for electrospray thrusters," *Journal of Applied Physics*, Vol. 130, No. 14, 2021. https://doi.org/10.1063/5.0063476.

[20] Natisin, M. R., Zamora, H. L., McGehee, W. A., Arnold, N. I., Holley, Z. A., Holmes, M. R., and Eckhardt, D., "Fabrication and characterization of a fully conventionally machined, high-performance porous-media electrospray thruster," *Journal of Micromechanics and Microengineering*, Vol. 30, No. 11, 2020. https://doi.org/10.1088/1361-6439/abb8c3.

[21] Svensson, B., Holmén, G., and Burén, A., "Angular dependence of the ion-induced secondary-electron yield from solids," *Phys. Rev. B*, Vol. 24, 1981, pp. 3749–3755. https://doi.org/10.1103/PhysRevB.24.3749.

[22] Lozano, P. C., "Studies on the ion-droplet mixed regime in colloid thrusters," Ph.D. thesis, Massachusetts Institute of Technology, 2003. URL http://ssl.mit.edu/publications/theses/PhD-2003-Lozano-TovarPaulo.pdf.